

Two-channel pseudogap Kondo and Anderson models: Quantum phase transitions and non-Fermi liquids

Imke Schneider,¹ Lars Fritz,² Frithjof B. Anders,³ Adel Benlagha,¹ and Matthias Vojta¹

¹*Institut für Theoretische Physik, Technische Universität Dresden, 01062 Dresden, Germany*

²*Institut für Theoretische Physik, Universität zu Köln, Zùlpicher Straße 77, 50937 Köln, Germany*

³*Lehrstuhl für Theoretische Physik II, Technische Universität Dortmund, Otto-Hahn-Str. 4, 44221 Dortmund, Germany*

(Dated: June 15, 2018)

We discuss the two-channel Kondo problem with a pseudogap density of states, $\rho(\omega) \propto |\omega|^r$, of the bath fermions. Combining both analytical and numerical renormalization group techniques, we characterize the impurity phases and quantum phase transitions of the relevant Kondo and Anderson models. The line of stable points, corresponding to the overscreened non-Fermi liquid behavior of the metallic $r = 0$ case, is replaced by a stable particle-hole symmetric intermediate-coupling fixed point for $0 < r < r_{\max} \approx 0.23$. For $r > r_{\max}$, this non-Fermi liquid phase disappears, and instead a critical fixed point with an emergent spin-channel symmetry appears, controlling the quantum phase transition between two phases with stable spin and channel moments, respectively. We propose low-energy field theories to describe the quantum phase transitions, all being formulated in fermionic variables. We employ epsilon expansion techniques to calculate critical properties near the critical dimensions $r = 0$ and $r = 1$, the latter being potentially relevant for two-channel Kondo impurities in neutral graphene. We find the analytical results to be in excellent agreement with those obtained from applying Wilson's numerical renormalization group technique.

I. INTRODUCTION

The two-channel Kondo effect represents a prime example of non-Fermi liquid behavior arising from a stable intermediate-coupling fixed point.¹ Theoretically, its physics is essentially understood, thanks to an exact solution by Bethe ansatz.^{2,3} In addition, boundary conformal field theory (CFT) has proved to be a powerful technique to study the low-energy properties of the multi-channel Kondo model⁴ allowing, in particular, the calculation of exact asymptotic Green's functions.⁵ CFT techniques have also been used to calculate exact crossover Green's functions.⁶ Further, by means of Abelian bosonization and subsequent re-fermionization it has been possible to map the two-channel Kondo problem onto a resonant-level model which reduces to a free fermion form for a particular value of exchange anisotropy.⁷

On the experimental side, a number of heavy-fermion materials, displaying deviations from Fermi-liquid behavior, have been speculated to realize two-channel Kondo physics arising from non-Kramers doublet ground states of U or Pr ions.^{8–10} However, to our knowledge, there is no unambiguous verification of these proposals. Consequently, various attempts were made to realize the two-channel Kondo effect in nanostructures, and indeed success was reported¹¹ for a setup of a semiconductor quantum dot coupled to two reservoirs.¹² Very recently, signatures of two-channel Kondo behavior of magnetic adatoms on graphene have been reported,¹³ and this motivates to discuss two-channel Kondo impurities in non-metallic hosts. In particular, neutral graphene realizes a pseudogap density of states (DOS), $\rho(\omega) \propto |\omega|^r$ with $r = 1$, at low energies.

The single-channel pseudogap Kondo problem has been studied extensively in the context of Kondo impurities in unconventional superconductors. The main dif-

ference to the familiar metallic Kondo problem¹⁴ is the absence of screening at small Kondo coupling J , leading to a quantum phase transition upon increasing J .^{15–19} The universality class of this phase transition changes as function of r ,¹⁹ and the relevant low-energy field theories have been worked out in detail in Refs. 20,21.

Although two-channel Kondo physics has been speculated about in the context of graphene,²² the two-channel pseudogap Kondo model has received little attention. A central question is about the fate and character of the non-Fermi-liquid phase at finite r . To our knowledge, the only study of the model has been reported in a brief section of Ref. 19, but there only numerical results were given for small bath exponents r .²³

The purpose of this paper is to close this gap: We shall investigate the two-channel Kondo and Anderson models with a pseudogap DOS in some detail, using both analytical and numerical renormalization group (RG) techniques. Our main findings for the two-channel Kondo model are:

(A) The overscreened non-Fermi liquid (NFL) phase of the metallic two-channel Kondo model¹⁴ survives for $0 < r < r_{\max} \approx 0.23$, albeit with an important modification: It is no longer represented by a *line* of NFL fixed points (where particle-hole (p-h) asymmetry is marginal), but instead there is only an isolated stable p-h symmetric NFL fixed point, i.e., p-h asymmetry is irrelevant for $r > 0$.²³ Furthermore, this stable NFL phase is only reached for Kondo couplings larger than a critical coupling, i.e., a boundary quantum phase transition emerges between a local-moment phase with an unscreened spin moment and the NFL phase. In contrast, for $r > r_{\max}$ the NFL fixed point disappears, leaving only two stable phases with unscreened spin or channel (i.e. flavor) moment, respectively, which are separated by a quantum phase transition.

(B) The two-channel pseudogap Kondo physics for both $r \lesssim 1$ and $r \geq 1$ can be fully understood in the language of the two-channel Anderson model, by virtue of a generalization of the approach presented in Ref. 21. The low-energy field theory describing the quantum phase transition between the phases with free spin and flavor moments is given by a level crossing of a spin doublet and a flavor doublet minimally coupled to conduction electrons. Similar to the single-channel pseudogap Kondo problem, $r = 1$ is found to play the role of an upper-critical dimension, where the hybridization is marginal. For $r > 1$, the transition is a level crossing with perturbative corrections, whereas a non-trivial critical fixed point emerges for $r < 1$. This fixed point is shown to display an emergent spin-channel Z_2 symmetry. As in the single-channel case, none of the quantum phase transitions is described by a Landau-Ginzburg-Wilson-type theory of a bosonic order parameter, instead all are “fermionic” in nature.

The following subsection gives a more detailed summary of our results.

A. Summary of results

The two-channel Kondo model with a pseudogap host density of states can be written as $\mathcal{H} = \mathcal{H}_K + \mathcal{H}_b$, with

$$\begin{aligned} \mathcal{H}_K &= \sum_i \left[J_K \vec{S} \cdot c_{i\sigma}^\dagger(0) \vec{\tau}_{\sigma\sigma'} c_{i\sigma'}(0) + V_0 c_{i\sigma}^\dagger(0) c_{i\sigma}(0) \right] (1) \\ \mathcal{H}_b &= \sum_i \int_{-\Lambda}^{\Lambda} dk |k|^r k c_{ki\sigma}^\dagger c_{ki\sigma}. \end{aligned}$$

Here, we have represented the bath, \mathcal{H}_b , by linearly dispersing chiral fermions $c_{ki\sigma}$, where $i = 1, 2$ is the channel index. \vec{S} is a spin-1/2 SU(2) spin, $\vec{\tau}$ is the vector of Pauli matrices, summation over repeated spin indices σ is implied, and $c_{i\sigma}(0) = \int dk |k|^r c_{ki\sigma}$ is the conduction electron operator at the impurity site. The spectral density of the $c_{i\sigma}(0)$ fermions follows the power law $|\omega|^r$ below the ultra-violet (UV) cutoff Λ ; details of the density of states at high energies are irrelevant for the discussion in this paper. In addition to the Kondo coupling J_K , we have also included a potential scatterer of strength V_0 at the impurity site which will be used to tune p-h asymmetry. (An asymmetry of the high-energy part of the DOS would have a net effect similar to non-zero V_0 ; for simplicity we will assume in the following that the DOS is p-h symmetric.)

As we shall show below, a comprehensive analysis requires to consider – in addition to the two-channel Kondo model – the two-channel Anderson model, commonly written as $\mathcal{H} = \mathcal{H}_A + \mathcal{H}_b$ with⁸

$$\begin{aligned} \mathcal{H}_A &= \varepsilon_s \sum_{\sigma} |\sigma\rangle\langle\sigma| + \varepsilon_q \sum_i |i\rangle\langle i| \quad (2) \\ &+ g_0 \sum_{k\sigma i} (|\sigma\rangle\langle i| c_{ki\sigma} + \text{H.c.}) + V_0 \sum_{\sigma i} c_{i\sigma}^\dagger(0) c_{i\sigma}(0). \end{aligned}$$

Here, the isolated impurity has four states, i.e., a spin doublet $|\sigma\rangle = |\uparrow\rangle, |\downarrow\rangle$ and a channel doublet $|i\rangle = |1\rangle, |2\rangle$. Their mass difference, $\varepsilon_0 \equiv \varepsilon_s - \varepsilon_q$, will play a role as a tuning parameter of the quantum phase transition.

For a given value of the bath exponent r , the two-channel pseudogap Kondo and Anderson models display common RG fixed points. The phase diagram and critical behavior depend on r , with $r = 0$, $r = r_{\max}$, and $r = 1$ marking qualitative changes and playing the role of critical “dimensions”. In the following, we describe our central results for the phase diagrams and RG flows, which are partially consistent²³ with the ones reported in Ref. 19. The qualitative behavior is visualized in the RG flow diagrams in Fig. 1 for the two-channel Kondo model and Fig. 2 for the two-channel Anderson model, respectively. In the latter case, a cut through the RG flow at $V_0 = 0$ is shown.

The metallic case $r = 0$, has been studied extensively, and a line of infrared stable NFL fixed points governs the behavior at any finite coupling – this is the well-known two-channel (or overscreened) Kondo effect. In the two-channel Anderson model, this line of fixed points can be accessed by varying ε_0 , i.e., initial parameters with different ε_0 flow to different fixed points along this line²⁵ – note that this flow leaves the $v = 0$ plane for $\varepsilon \neq 0$ (dashed in Fig. 2, all symbols denote the renormalized coupling parameter).

For positive r with $0 < r < r_{\max}$, the line of stable NFL fixed points collapses to an isolated p-h symmetric NFL fixed point. In addition, the local-moment fixed point (LM) of an unscreened spin moment now becomes stable. In the language of the Kondo model, LM corresponds to $j = v = 0$, while in the Anderson model it corresponds to $\varepsilon = -\infty$, $g = 0$. The phase transition between LM and NFL is controlled by a critical p-h symmetric fixed point (SCR); note that this p-h symmetric fixed point is located outside the $v = 0$ plane for the Anderson model shown in Fig. 2. As $r \rightarrow 0$ SCR approaches LM and the critical behavior of SCR is perturbatively accessible for small Kondo coupling J_K . The phase diagram of the Anderson model is mirror symmetric, i.e., there exists also an unscreened channel (or flavor) local-moment fixed point LM' at $\varepsilon = \infty$, $g = 0$ ²⁴ and a corresponding critical intermediate-coupling fixed point SCR' at positive ε .

As $r \rightarrow r_{\max}$ SCR approaches NFL, and the two fixed points disappear for $r > r_{\max}$. In the p-h symmetric Kondo model, this implies that the flow is towards LM for any value of j , but for large asymmetries, LM' may be reached.²⁴ In the Anderson model, the hybridization g remains relevant at $\varepsilon = 0$ for $r_{\max} < r < 1$, but the flow is towards a single unstable intermediate coupling fixed point (ACR) in the $v = 0$ plane, i.e., ACR is p-h asymmetric, but is invariant under the Z_2 transformation (4). At finite coupling, the transition between the two stable fixed points LM and LM' is controlled by ACR.

Finally, as $r \rightarrow 1$ ACR moves toward $g \rightarrow 0$ and for $r \geq 1$ the phase transition becomes a level crossing with

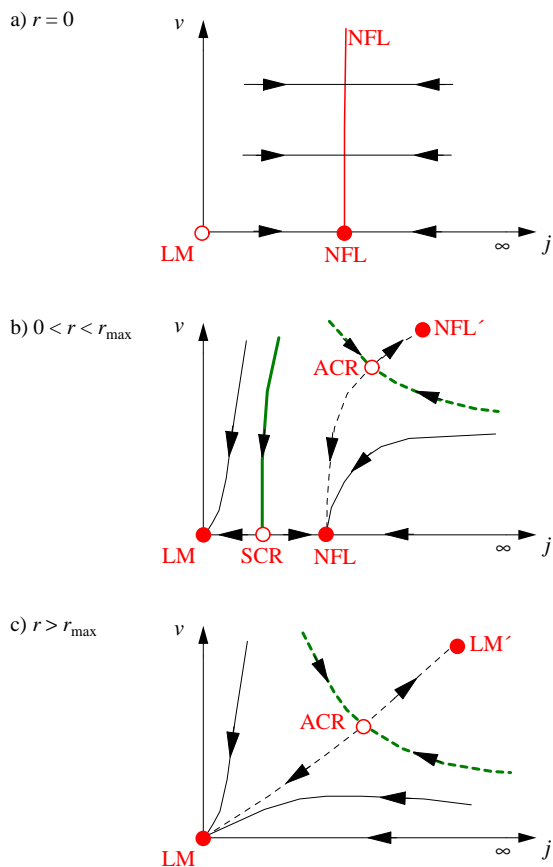


FIG. 1: Schematic RG flow diagrams for the two-channel Kondo model with a pseudogap DOS, $\rho(\omega) \propto |\omega|^r$. The horizontal axis denotes the renormalized Kondo coupling j , the vertical axis is the renormalized potential scattering v , representing particle-hole asymmetry. Dashed flow lines symbolize a flow out of the plane shown here. The thick lines correspond to continuous boundary phase transitions; the full (open) circles are stable (unstable) fixed points. a) $r=0$, i.e., the familiar metallic case. For any finite j the flow is towards the line of NFL fixed points, describing two-channel non-Fermi liquid behavior. b) $0 < r < r_{\max}$: P-h asymmetry is irrelevant in the NFL phase, such that the line of fixed points is replaced by a single p-h symmetric NFL fixed point. The local-moment fixed point LM is stable and separated from NFL by a p-h symmetric critical SCR fixed point. For $r \rightarrow 0$ ($r \rightarrow r_{\max}$), SCR approaches LM (NFL). Depending on microscopic details, a second NFL' phase may be reached at large couplings and asymmetries, separated by a critical ACR fixed point, see text. c) $r \geq r_{\max}$: The NFL phase disappears, and the only phase transition is between LM and LM', the latter representing a free channel (i.e. flavor) moment. This transition is controlled by ACR. Note that the character of this transition changes at $r = 1$, where ACR merges with FImp, see text.

perturbative corrections, controlled by the free impurity fixed point (FImp) at $\varepsilon = 0, g = 0$.

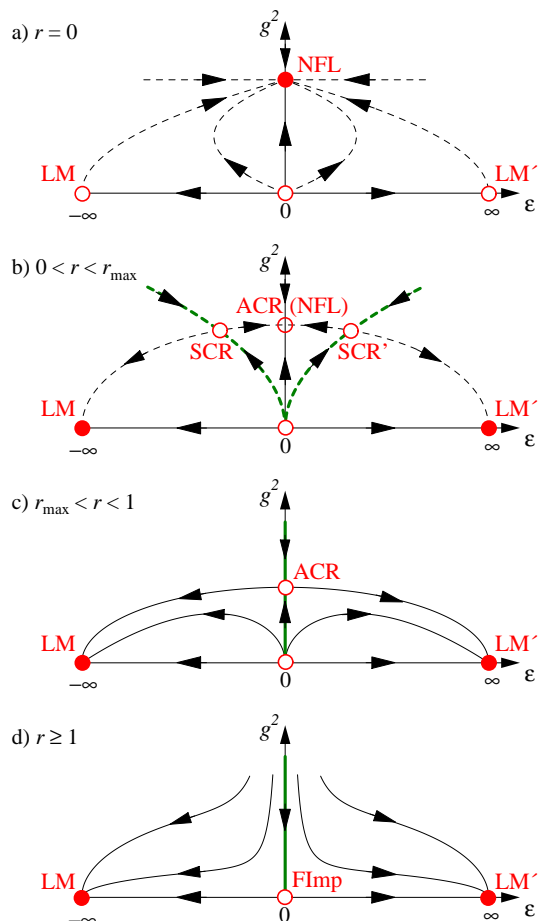


FIG. 2: As Fig. 1, but for the two-channel Anderson model. The horizontal axis denotes the energy difference ε between spin and flavor impurity levels, the vertical axis is the renormalized hybridization g . The diagrams represent cuts, taken at $v = 0$, through the full RG flow. The flow diagrams are mirror-symmetric by virtue of the Z_2 transformation (4). a) $r = 0$. The line of NFL fixed points, describing two-channel non-Fermi liquid behavior crosses the $v = 0$ plane at $\varepsilon = 0$. b) $0 < r < r_{\max}$: The fixed points LM, LM' are stable, corresponding to unscreened spin and flavor moments, respectively. Within the $v = 0$ plane, NFL is replaced by ACR, whereas two isolated p-h symmetric NFL/NFL' fixed points exist outside this plane. The transitions to NFL/NFL' are controlled by the p-h symmetric SCR/SCR' fixed points (located outside the $v = 0$ plane). c) $r_{\max} \leq r < 1$: g is still relevant at $\varepsilon = 0$. However, NFL is now replaced by a single unstable fixed point (ACR) located in the $v = 0$ plane. At finite g , the transition between the two stable fixed points LM and LM' is controlled by ACR. d) $r \geq 1$: g is irrelevant, and the only transition is a level crossing (with perturbative corrections) occurring at $g = \varepsilon = 0$, i.e., at the free-impurity fixed point (FImp).

B. Outline

The bulk of this paper is organized as follows: We start in Sec. II by discussing the relevant impurity models,

suitably generalized to higher degeneracies, along with their underlying symmetries. In Sec. III we present selected results from Wilson's numerical renormalization group (NRG) for the two-channel pseudogap Anderson and Kondo models which illustrate the content of the flow diagrams in Figs. 1 and 2. In particular, we show properties of the non-trivial intermediate-coupling fixed points as function of the bath exponent r . Secs. IV and V are devoted to the epsilon expansion studies of the critical fixed points, using the variables of the Kondo model (Sec. IV) and that of the Anderson model (Sec. V). The latter provide access to the physics near the upper-critical dimension $r = 1$. Concluding remarks will close the paper. A discussion of the Majorana representation of the two-channel Kondo problem and its fate in the presence of a pseudogap DOS is relegated to the appendix.

II. MODELS, SYMMETRIES, AND MAPPINGS

A. Anderson model

The two-channel Anderson model can be understood as describing the level crossing between two impurity doublets – one spin doublet and one channel (i.e. flavor) doublet – coupled to conduction electrons via a hybridization term. The model features an $SU(2)_{\text{spin}} \times SU(2)_{\text{flavor}}$ symmetry. This can be straightforwardly generalized to $SU(N)_{\text{spin}} \times SU(K)_{\text{flavor}}$ symmetry, where N is the number of spin degrees of freedom and K the number of flavors. The Hamiltonian can be written as:

$$\begin{aligned} \mathcal{H}_A = & \mathcal{H}_b + \varepsilon_s \sum_{\sigma} |\sigma\rangle\langle\sigma| + \varepsilon_q \sum_{\alpha} |\bar{\alpha}\rangle\langle\bar{\alpha}| \\ & + g_0 \sum_{k\alpha\sigma} (|\sigma\rangle\langle\bar{\alpha}| c_{k\alpha\sigma} + \text{H.c.}) + V_0 \sum_{\alpha\sigma} c_{\alpha\sigma}^{\dagger}(0) c_{\alpha\sigma}(0) \end{aligned} \quad (3)$$

Here, the conduction electrons $c_{k\alpha\sigma}$ transform under a fundamental representation of $SU(N)$ and $SU(K)$ and carry the corresponding spin σ and flavor α indices. $\bar{\alpha}$ indicates a transformation behavior according to the conjugate representation. For $N = 2$, $K = 1$, the Hamiltonian in Eq. (3) describes the single-channel Anderson model in the limit of infinite Coulomb repulsion ($U = \infty$), studied using RG in Ref. 21. In case of a metallic host, $r = 0$, the multi-channel Anderson model is integrable and has been solved using the Bethe Ansatz^{25–27} and the numerical RG method.²⁸

The metallic two-channel Anderson model, i.e. $N = 2$, $K = 2$, has been proposed as a model for the observed non-Fermi liquid behavior of the heavy-fermion superconductor UBe_{13} .²⁹ In this scenario, the $5f^2$ ground state of the U ion is identified as the Γ_3 non-magnetic quadrupolar doublet, while the first excited state is the $5f^3$ Γ_7 magnetic doublet.⁸ This then can promote a quadrupolar Kondo effect where the quadrupolar doublet is quenched by the hybridization with Γ_8 conduction electrons which carry both magnetic and quadrupolar de-

grees of freedom.⁹ In particular, since the energy difference between the two doublets appears to be small, a mixed valence state is likely requiring the study of the full Anderson model.³⁰ Consequently, the model (3) with a pseudogap DOS is of potential relevance not only to two-channel impurities in graphene, but also to quadrupolar Kondo impurities in unconventional superconductors.

The Anderson model (3) is *not* particle-hole symmetric for any value of V_0 , due to the asymmetric structure of the impurity. However, p-h symmetry is dynamically restored for $0 < r < r_{\text{max}}$ both inside the NFL/NFL' phases and at the critical SCR/SCR' fixed points, see Fig. 1.

Interestingly, for $N = K$ and a p-h symmetric bath, the Anderson model displays a spin-channel symmetry, i.e., is invariant under the combined transformation

$$\begin{aligned} |\sigma\rangle & \leftrightarrow |\bar{\alpha}\rangle \\ c_{k\alpha\sigma} & \leftrightarrow c_{k\alpha\sigma}^{\dagger} \\ \varepsilon_0 & \leftrightarrow -\varepsilon_0 \\ V_0 & \leftrightarrow -V_0 \end{aligned} \quad (4)$$

Here, the spin-carrying impurity states are transformed into the flavor-carrying states and vice versa, i.e., the two $SU(N)$ sectors are interchanged, together with a p-h transformation.

B. Kondo models

The Anderson model (3) has two Kondo limits. On the one hand, for $\varepsilon_0 = \varepsilon_s - \varepsilon_q \rightarrow -\infty$ it maps to a K -channel $SU(N)_{\text{spin}}$ -Kondo model, where a spinful impurity is coupled to K channels of conduction electrons. For $N = 2$ the Hamiltonian reads

$$\begin{aligned} \mathcal{H}_K = & \mathcal{H}_b + J_K \vec{S} \cdot \sum_{\alpha\sigma\sigma'} c_{\alpha\sigma}^{\dagger}(0) \vec{\tau}_{\sigma\sigma'} c_{\alpha\sigma'}(0) \\ & + V_0 \sum_{\alpha\sigma} c_{\alpha\sigma}^{\dagger}(0) c_{\alpha\sigma}(0) \end{aligned} \quad (5)$$

where \vec{S} is a spin-1/2 $SU(2)$ spin and $\sigma, \sigma' = \uparrow, \downarrow$. For $N > 2$ the impurity spin is in a fundamental representation of $SU(N)$. The parameters of the Kondo model (5) are related to that of the $V_0 = 0$ Anderson model (3) through:

$$J_K = NV_0 = \frac{g_0^2}{|\varepsilon_0|}. \quad (6)$$

The Kondo limit is reached by taking $\varepsilon_0 \rightarrow -\infty$, $g_0 \rightarrow \infty$, keeping J_K fixed. Note that a potential scattering term is always generated.

On the other hand, for $\varepsilon_0 \rightarrow +\infty$ the Anderson model can be mapped to a N -channel $SU(K)_{\text{flavor}}$ -Kondo model, where \vec{S} represents a $SU(K)$ impurity which is screened by the N spin degrees of freedom of the conduction electrons. Such multi-channel flavor Kondo effect is relevant, e.g., to the charging process of a quantum box,

where the flavor degree of freedom is taken by the physical charge.^{31,32}

We note that the multi-channel Kondo model cannot be obtained by a Schrieffer-Wolff transformation from any standard Anderson model (i.e., written with free-electron operators and local Coulomb interaction).

C. Large- N limit

The $SU(N)$ multi-channel Kondo model can be solved in a dynamic large- N limit for both fully symmetric (bosonic) and fully antisymmetric (fermionic) representations of $SU(N)$.³³ The fermionic version of this solution, with $K = \gamma N$ and $K, N \rightarrow \infty$, has been generalized to the pseudogap case.³⁴ The large- N phase diagram, Fig. 1 of Ref. 34, is similar to that of the $N = K = 2$ case, i.e., the overscreened non-Fermi liquid phase survives for small r , where it is reached for a certain range of couplings only, while this phase disappears for larger $r \lesssim 1$. Also, all leading anomalous dimensions vanish for $r > 1$.

Two qualitative differences between the large- N scenario and $N = K = 2$ are worth noting: (i) The critical “dimension” r_{\max} of $N = K = 2$ splits into two in the large- N limit, with their values and the detailed behavior depending upon the value of γ . (ii) The quantum phase transitions in the large- N limit are governed by *lines* of fixed points, with continuously varying exponents as function of the particle-hole asymmetry, in contrast to the isolated critical fixed points SCR and ACR in Figs. 1 and 2. This implies that the scaling dimension of V_0 vanishes at criticality as $N \rightarrow \infty$, rendering the large- N limit partially singular. We therefore refrain from a detailed discussion of the models (3) and (5) for large N .

D. Observables

In the bulk of the paper, we will focus on a few important observables which characterize the phases and phase transitions of the impurity models under consideration. Those include the correlation-length exponent, the impurity entropy, various susceptibilities, and the conduction-electron T matrix (or impurity spectral function). Their definition is standard, and we refer the reader to Refs. 19,21,35–37 for a detailed exposition. Here we only summarize a few key aspects.

Spin susceptibilities, $\chi^{(\text{spin})}$, are obtained by coupling external magnetic fields both to the bulk and impurity degrees of freedom as explained in detail in Ref. 37. For the impurity part, here, this reads

$$-H_{\text{imp},i} |\sigma\rangle \lambda_{\sigma\sigma'}^i \langle\sigma'|, \quad (7)$$

where $H_{\text{imp},i}$ is the magnetic field coupling to the impurity spin, while the $\lambda_{\sigma\sigma'}^i$, with $i = 1, N - 1$ are generators of $SU(N)$. In the following, we exploit the $SU(N)$

symmetry and only evaluate the corresponding susceptibility tensor in the 1-direction choosing the representation $\lambda_{\sigma,\sigma'}^1 = \frac{1}{2}(\delta_{\sigma,1}\delta_{\sigma',1} - \delta_{\sigma,2}\delta_{\sigma',2})$.³⁸ We proceed as usual by calculating the magnetic susceptibilities via the corresponding linear response functions. Note that the impurity susceptibility is composed of

$$\chi_{\text{imp}}(T) = \chi_{\text{imp,imp}} + 2\chi_{\text{b,imp}} + (\chi_{\text{b,b}} - \chi_{\text{b,b}}^0), \quad (8)$$

where $\chi_{\text{imp,imp}}$ is the response to H_{imp} , $\chi_{\text{b,b}}$ measures the bulk response to the field applied to the bulk, $\chi_{\text{b,imp}}$ are the cross terms, and $\chi_{\text{b,b}}^0$ denotes the bulk response in the absence of the impurity. Flavor susceptibilities, $\chi^{(\text{flavor})}$, can be defined in the Anderson model in analogy to the spin susceptibilities (i.e., with $\sigma \rightarrow \alpha$).

Owing to symmetries, the total magnetization in both the spin and flavor sectors is conserved. This implies that the impurity contributions to the spin and flavor susceptibilities, $\chi_{\text{imp}}^{(\text{spin})}$ and $\chi_{\text{imp}}^{(\text{flavor})}$, do not acquire anomalous exponents at the intermediate-coupling fixed points, but instead obey Curie laws with (in general) fractional prefactors. In contrast, the local spin and flavor susceptibilities follow anomalous power laws, $\chi_{\text{loc}}^{(\text{spin})} \propto T^{-1+\eta_{\chi}^{(\text{spin})}}$ and $\chi_{\text{loc}}^{(\text{flavor})} \propto T^{-1+\eta_{\chi}^{(\text{flavor})}}$, with universal r -dependent exponents η_{χ} . We note that a direct calculation of both susceptibilities is only possible in the Anderson model, as the Kondo limit suppresses the local piece of one of the susceptibilities. To shorten notation, we employ the convention $\chi \equiv \chi^{(\text{spin})}$ and $\eta_{\chi} \equiv \eta_{\chi}^{(\text{spin})}$ in the following.

Similar to $T\chi_{\text{imp}}^{(\text{spin,flavor})}$, the impurity entropy approaches a universal fractional value as $T \rightarrow 0$. The conduction-electron T matrix, on the other hand, follows an anomalous power law similar to the local susceptibility, $T(\omega) \propto \omega^{-1+\eta_T}$.

At the non-Fermi-liquid fixed point of the familiar metallic two-channel Kondo model ($r = 0$), power laws are replaced by logs, $\chi_{\text{loc}}, \chi_{\text{imp}} \propto \ln 1/T$ – this also implies that the prefactor of the leading Curie term in χ_{imp} vanishes due to an exact compensation.

III. SELECTED NUMERICAL RESULTS

The NRG technique³⁹ is ideally suited to study properties of quantum impurity models, including non-Fermi liquid phases and quantum phase transitions. Initial NRG results for the two-channel pseudogap Kondo model were shown in Ref. 19. Here we extend and complement this early analysis by NRG results for the two-channel ($N = K = 2$) Anderson model. We perform explicit calculations for a bath density of states $\rho(\omega) = (1+r)/(2D)|\omega/D|^r \Theta(D^2 - \omega^2)$ with $D = 1$. Unless otherwise noted, we employ NRG parameters³⁹ $\Lambda = 6$ and $N_s = 600$.

The qualitative behavior of the two-channel Anderson model is summarized in the flow diagram in Fig. 2. In addition to the stable LM/LM' phases, these flow di-

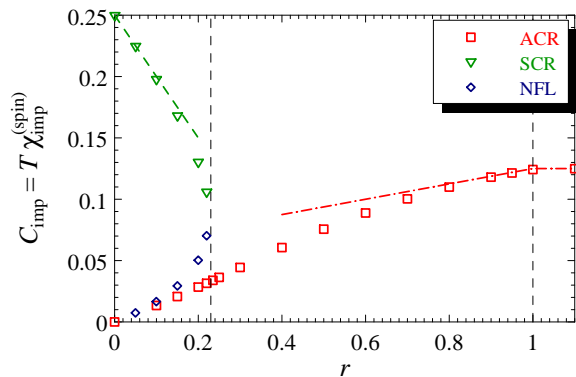


FIG. 3: NRG for the impurity susceptibility, $T\chi_{\text{imp}}^{(\text{spin})}$, at the intermediate-coupling fixed points ACR (\square), SCR (\triangle), and NFL (\diamond). Also shown are the results from the renormalized perturbation theory of the Kondo model, which allows to access SCR near $r = 0$ [Sec. IV, Eq. (14), dashed], and that of the Anderson model, appropriate for ACR for $r \lesssim 1$ [Sec. V, Eq. (49), dash-dot]. The SCR data have been partially taken from Ref. 19. The vertical dashed lines indicate the critical dimensions $r = r_{\text{max}}$ and $r = 1$.

agrams feature three non-trivial fixed points: the stable NFL/NFL' fixed points and the critical fixed points SCR/SCR' and ACR. Some of their key properties are summarized in Figs. 3 and 4, which show the numerically determined impurity contributions to the spin susceptibility and the entropy, respectively, together with analytical results obtained from the epsilon expansion of Secs. IV and V. These plots nicely show that NFL and SCR approach each other as $r \rightarrow r_{\text{max}}$, while ACR evolves continuously near r_{max} . The fixed-point properties also show that SCR approaches LM as $r \rightarrow 0$, with $T\chi_{\text{imp}} \rightarrow 1/4$ and $S_{\text{imp}} \rightarrow \ln 2$, and ACR approaches FImp as $r \rightarrow 1$, with $T\chi_{\text{imp}} \rightarrow 1/8$ and $S_{\text{imp}} \rightarrow \ln 4$. Further, the stable NFL fixed point follows $T\chi_{\text{imp}} \rightarrow 0$

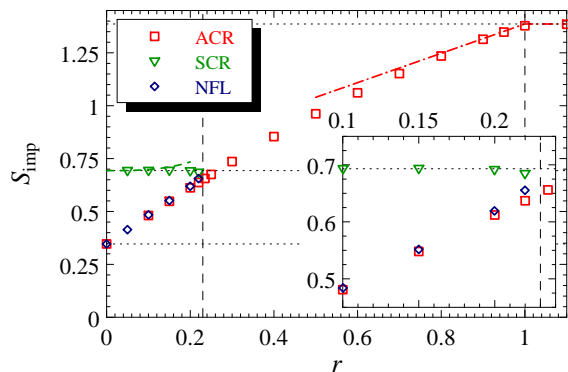


FIG. 4: As Fig. 3, but for the impurity entropy S_{imp} . The perturbative expansions are in Eq. (15) (dashed) and Eq. (53) (dash-dot). The dotted horizontal lines correspond to $S_{\text{imp}} = 0.5 \ln 2$, $\ln 2$, and $\ln 4$. The inset shows a zoom onto the region $r \lesssim r_{\text{max}}$.

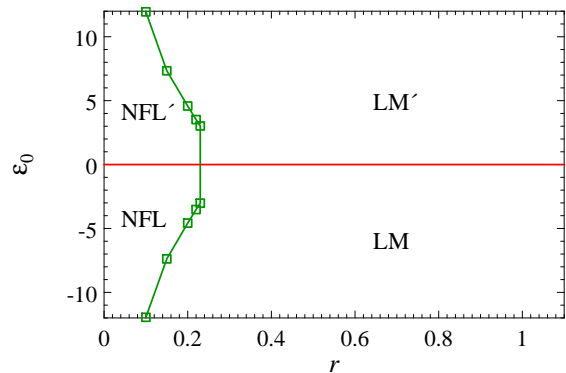


FIG. 5: Phase diagram of the two-channel Anderson model as function of the energy difference ε_0 and the bath exponent r , keeping $g_0^2 = 4$ fixed. The discontinuous change at $r = r_{\text{max}}$ is apparent.

and $S_{\text{imp}} \rightarrow 0.5 \ln 2$ as $r \rightarrow 0$ – the well-known properties of the metallic two-channel Kondo problem.

The disappearance of both NFL and SCR upon increasing r beyond r_{max} implies a *discontinuous* evolution of the phase diagram as function of r . In Fig. 5 we present a cut through the phase diagram of the Anderson model at fixed g_0 which illustrates this fact. We note that such a discontinuous evolution occurs if a stable intermediate-coupling fixed point disappears (here NFL); in contrast, if a trivial fixed point changes its nature from stable to unstable, the evolution is continuous, like in the single-channel pseudogap Kondo model.

The correlation-length exponents ν are displayed in Fig. 6, illustrating that $r = 0$ and r_{max} play the role of lower-critical dimensions for the p-h symmetric transition controlled by SCR, with $\nu \rightarrow \infty$, whereas $r = 1$ is

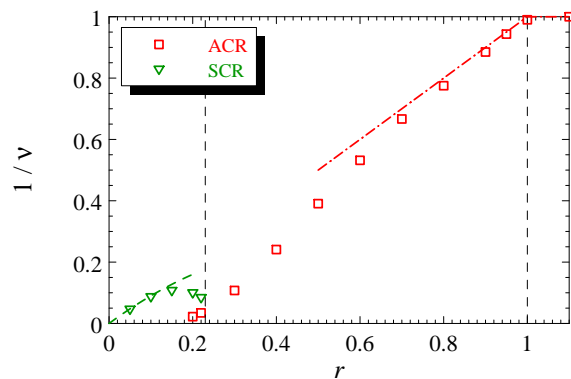


FIG. 6: Inverse correlation-length exponent $1/\nu$ obtained from NRG for the ACR (\square) and SCR (\triangle) critical points, together with the analytical RG results from the expansions in r [Sec. IV, Eq. (12), dashed] and in $(1-r)$ [Sec. V, Eq. (38), dash-dot]. Note that ν of ACR becomes very large for small r – this corresponds to the extremely slow flow from ACR to NFL for $0 < r < r_{\text{max}}$.

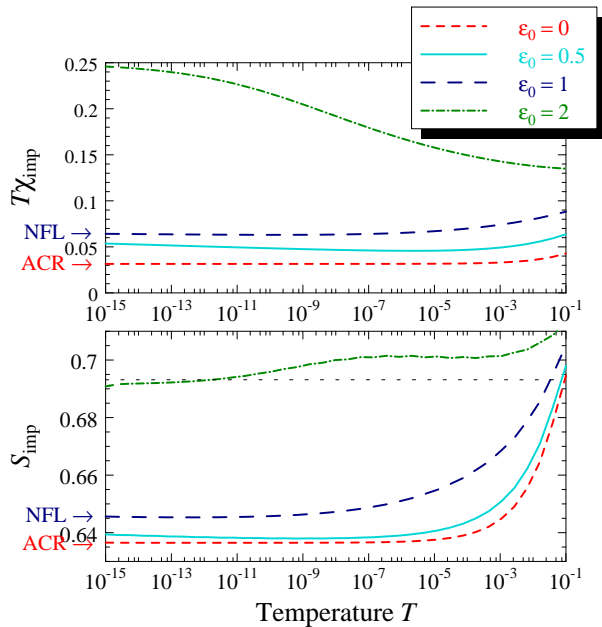


FIG. 7: NRG results for a) the impurity susceptibility $T\chi_{\text{imp}}$ and b) the impurity entropy S_{imp} of the two-channel Anderson model at $r = 0.22$. Parameter values are $g_0^2 = 2$ and $\varepsilon_0 = 0$ (dashed), 0.5 (solid), 1 (long-dash), 2 (dash-dot). Both $\varepsilon_0 = 0.5$ and 1 are located in the NFL phase while $\varepsilon_0 = 2$ corresponds to the LM phase. The $\varepsilon_0 = 0.5$ curves show the flow from ACR to NFL upon lowering T , where in particular the impurity entropy *increases* along the RG flow. (The flow is too slow to reach its fixed point within the accessible temperature range.)

the upper-critical dimension of the ACR transition, with $\nu = 1$ for all $r > 1$ (and logarithmic corrections at $r = 1$).

Fig. 7 shows the temperature evolution of both $T\chi_{\text{imp}}$ and S_{imp} for $r = 0.22$, i.e., slightly below r_{max} . Here, the flow from ACR to NFL (compare Fig. 1b) is nicely visible at $\varepsilon_0 = 0.5$ where both $T\chi_{\text{imp}}$ and S_{imp} increase along the RG flow. (The large value of ν at ACR renders the flow very slow.) Remarkably, the fact $S_{\text{ACR}} < S_{\text{NFL}}$ violates so-called g -theorem,⁴⁰ which states that the impurity entropy should decrease along the flow. As this theorem applies to conformally invariant systems only, we conclude that the fixed points under consideration are not described by a conformally invariant theory. (The same conclusion can be drawn for the quantum phase transitions of the single-channel pseudogap Kondo problem, see Ref. 21. Also, such “uphill flow” may occur in models with long-range interactions, see e.g. Ref. 41.)

IV. WEAK-COUPLING EXPANSION FOR THE MULTI-CHANNEL KONDO MODEL

In this section we review the standard weak-coupling expansion⁴² for the multi-channel SU(2)-Kondo model in Eq. (5), extended to a pseudogapped bath density of

states.^{15,19} As we show below, this expansion captures the properties of the critical fixed point SCR at small r . In principle, it also allows to access the stable NFL fixed point, but this requires a particular limit of large K which does not allow to extract quantitative results for the $K = 2$ case of interest.

RG equations can be derived, e.g., using the field-theoretic scheme^{43,44} where logarithmic divergencies, occurring for $r = 0$, are replaced by poles in r by means of “dimensional” regularization. Doing so, r will only enter in the bare scaling dimension of the couplings. To two-loop order, the equations for the renormalized couplings j and v read

$$\beta(j) = rj - j^2 + \frac{K}{2}j^3, \quad (9)$$

$$\beta(v) = rv,$$

where K is the number of equivalent screening channels. Importantly, there is no renormalization of v , a result which persists to higher orders.

Apart from the LM fixed point, $j = v = 0$, the function $\beta(j)$ in Eq. (9) yields two further zeros, given by $j = (1 \pm \sqrt{1 - 2Kr})/K$. The smaller one corresponds to an infrared unstable fixed point at

$$j^* = r + \frac{K}{2}r^2 + \mathcal{O}(r^3), \quad v^* = 0 \quad (10)$$

which can be perturbatively controlled for $r \rightarrow 0$ and any K . We label this fixed point by SCR. As $r \rightarrow 0$ SCR approaches LM. The larger zero predicts an infrared stable fixed point at

$$j^* = \frac{2}{K} - r - \frac{K}{2}r^2 + \mathcal{O}(r^3), \quad v^* = 0. \quad (11)$$

Strictly speaking, this fixed point is perturbatively accessible only if the limits $r \rightarrow 0$ and $K \rightarrow \infty$ are either taken in this order (this corresponds to $r = 0$) or together such that Kr is kept fixed. For $r = 0$, where v is marginal, this zero of $\beta(j)$ is commonly associated with the line of stable non-Fermi liquid fixed points of the multi-channel Kondo model, which exists for all $K \geq 2$. For $r > 0$ now v becomes irrelevant, in agreement with our numerical results²³ which show that the NFL line of fixed points shrinks to a single p-h symmetric NFL fixed point, Fig. 1.

A. Observables near criticality

The properties of the p-h symmetric critical fixed point SCR, existing for $0 < r < r_{\text{max}}$, can be determined in analogy to the single-channel case, with explicit calculations given e.g. in Ref. 37. Expanding the beta function (9) around the fixed point value (10) yields the correlation length exponent ν :

$$\frac{1}{\nu} = r - \frac{K}{2}r^2 + \mathcal{O}(r^3). \quad (12)$$

The leading-order perturbative corrections to the impurity susceptibility and entropy are given by

$$\begin{aligned}\Delta(T\chi_{\text{imp}}) &= -\frac{Kj}{4}, \\ \Delta S_{\text{imp}} &= \frac{3\pi^2 \ln 2}{8} K j^2 r.\end{aligned}\quad (13)$$

Inserting the fixed-point value j^* (10) we obtain

$$T\chi_{\text{imp}} = \frac{1}{4}(1 - Kr) + \mathcal{O}(r^2), \quad (14)$$

$$S_{\text{imp}} = \ln 2 \left(1 + \frac{3\pi^2}{8} Kr^3 \right) + \mathcal{O}(r^5). \quad (15)$$

The anomalous exponent of the local susceptibility is given by $\eta_\chi = Kj^2$ to leading order, which evaluates to

$$\eta_\chi = Kr^2 + \mathcal{O}(r^3). \quad (16)$$

Finally, the T matrix exponent is $\eta_T = 1 - j$ (with no factor of K , as the T matrix describes the scattering of electrons from one specific channel), resulting in

$$\eta_T = 1 - r. \quad (17)$$

Note that this result is exact.²¹

V. HYBRIDIZATION EXPANSION FOR THE MULTI-CHANNEL ANDERSON MODEL

We now turn our attention to the multi-channel Anderson model. As we show below, the variables of the Anderson model will allow us to obtain an essentially complete understanding of the multi-channel pseudogap Kondo effect both for $r \lesssim 1$ and $r \geq 1$. A similar conclusion was reached for the single-channel case in Refs. 20,21, and – on a technical level – our work represents a generalization of the calculation for the infinite- U Anderson model in Ref. 21.

A. Trivial fixed points

For vanishing hybridization g_0 , the multi-channel Anderson model (3) features three trivial fixed points: for $\varepsilon_0 < 0$ the ground state is the spinful N -fold degenerate local-moment state (LM) and, analogously, for $\varepsilon_0 > 0$ it is the K -fold degenerate flavor local-moment state (LM'). In these cases the impurity entropy equals $\ln N$ and $\ln K$, respectively. For $\varepsilon_0 = 0$ there are $(N+K)$ degenerate impurity states, we refer to this as the free-impurity fixed point (FImp), with entropy $\ln(N+K)$. The impurity spin susceptibilities are

$$T\chi_{\text{imp}}^{(\text{spin})} = \begin{cases} \frac{1}{2N} & \text{LM} \\ \frac{1}{2(N+K)} & \text{FImp} \\ 0 & \text{LM}' \end{cases}. \quad (18)$$

The corresponding values of $T\chi_{\text{imp}}^{(\text{flavor})}$ follow via Eq. (4) from $\text{LM} \leftrightarrow \text{LM}'$. The hybridization term, g_0 , is irrelevant at LM and LM' for $r > 0$.

B. Hybridization expansion and upper critical dimension

In the following we perform an expansion around the FImp fixed point, i.e., around $\varepsilon_0 = 0$, $g_0 = 0$.

The impurity states are represented by bosonic operators $b_{\bar{\alpha}}^\dagger$ for $\alpha = 1, \dots, K$ and fermionic operators f_σ for $\sigma = 1, \dots, N$. Single occupancy of the localized levels is enforced by the Hilbert space constraint $\hat{Q} \equiv \sum_\alpha b_{\bar{\alpha}}^\dagger b_{\bar{\alpha}} + \sum_\sigma f_\sigma^\dagger f_\sigma = 1$ which will be implemented using a chemical potential $\lambda_0 \rightarrow \infty$. Observables are then calculated as^{45,46}

$$\langle \hat{O} \rangle = \lim_{\lambda_0 \rightarrow \infty} \frac{\langle \hat{Q} \hat{O} \rangle_{\lambda_0}}{\langle \hat{Q} \rangle_{\lambda_0}}, \quad (19)$$

where $\langle \dots \rangle_{\lambda_0}$ denotes the thermal expectation value in the presence of the chemical potential λ_0 .

Furthermore, we need to introduce chemical-potential counter-terms which cancel the shift of the critical point occurring in perturbation theory upon taking the limit of infinite UV cutoff. Technically, this shift arises from the real parts of the self-energies of the $b_{\bar{\alpha}}$ and f_σ particles. We introduce the counter-terms as additional chemical potential for the auxiliary particles,

$$\delta\lambda_b b_{\bar{\alpha}}^\dagger b_{\bar{\alpha}}, \quad \delta\lambda_f f_\sigma^\dagger f_\sigma. \quad (20)$$

The $\delta\lambda_{b,f}$ have to be determined order by order in an expansion in g_0 . Note that counter-term contributions in observables in general enter both numerator and denominator in Eq. (19).

In the path integral form the model (3) is written as

$$\begin{aligned}S = \int_0^\beta d\tau \left[\bar{f}_\sigma(\partial_\tau + \lambda_0 + \varepsilon_s + \delta\lambda_f) f_\sigma \right. \\ + \bar{b}_{\bar{\alpha}}(\partial_\tau + \lambda_0 + \varepsilon_q + \delta\lambda_b) b_{\bar{\alpha}} \\ + g_0 (\bar{f}_\sigma b_{\bar{\alpha}} c_{\alpha\sigma}(0) + \text{c.c.}) \\ \left. + \int_{-\Lambda}^\Lambda dk |k|^r \bar{c}_{k\alpha\sigma}(\partial_\tau + k) c_{k\alpha\sigma} \right], \quad (21)\end{aligned}$$

where λ_0 is the chemical potential enforcing the constraint exactly. Here, we implicitly sum over σ and α .

The model (21) shows a transition driven by variation of $\varepsilon_0 = \varepsilon_s - \varepsilon_q$. At the $\varepsilon_0 = g_0 = 0$ fixed point, tree level scaling analysis shows that

$$\dim[g_0] = \frac{1-r}{2} \equiv \bar{r}, \quad (22)$$

$$\dim[\varepsilon_0] = 1.$$

As in the single-channel model,^{20,21} this establishes the role of $r = 1$ as an upper-critical dimension where g_0 is marginal.

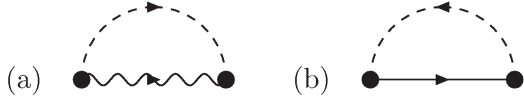


FIG. 8: Feynman diagrams entering the self energies up to quadratic order in g_0 . Full/dashed/wiggly lines denote $f_\sigma/c_\sigma/b_{\bar{\alpha}}$ propagators, the full dots are g_0 interaction vertices.

We perform a field-theoretical RG analysis using the minimal subtraction scheme.^{43,44} Renormalized fields and dimensionless couplings are introduced according to

$$f_\sigma = \sqrt{Z_f} f_{R\sigma}, \quad (23)$$

$$b_{\bar{\alpha}} = \sqrt{Z_b} b_{R\bar{\alpha}}, \quad (24)$$

$$g_0 = \frac{\mu^{\bar{r}} Z_g}{\sqrt{Z_f Z_b}} g, \quad (25)$$

where μ is the renormalization group energy scale. No renormalizations are needed for the bulk fermions as their self interaction is assumed to be irrelevant. The RG is conveniently performed at criticality, i.e. we assume that ε_0 is tuned to the critical line and set $\varepsilon_q = \varepsilon_s = 0$.

To determine the RG beta function $\beta(g)$ we evaluate the fermionic self-energy up to one-loop order

$$\Sigma_{f_\sigma}(i\omega_n) = K g^2 \frac{\mu^{2\bar{r}}}{\beta} \sum_{i\omega'_n} \int_{-\Lambda}^{\Lambda} dk |k|^r \frac{1}{i\omega'_n - k} \frac{1}{i\bar{\omega}_n - i\omega'_n} \quad (26)$$

corresponding to the diagram in Fig. 8a. Here, we have introduced the abbreviated notation $i\bar{\omega}_n = i\omega_n - \lambda_0$ for the Matsubara frequencies $i\omega_n = i\pi(2n+1)/\beta$. In the limit $\lambda_0 \rightarrow \infty$ and $\beta \rightarrow \infty$ we obtain

$$\Sigma_{f_\sigma}(i\omega_n) = K g^2 \mu^{2\bar{r}} \int_0^\Lambda d\epsilon \epsilon^r \frac{1}{i\bar{\omega}_n - \epsilon} \quad (27)$$

$$\approx -K g^2 \left(\mu^{2\bar{r}} \frac{\Lambda^r}{r} + i\bar{\omega}_n \frac{1}{2\bar{r}} \right). \quad (28)$$

An analogous expression is found for the bosonic self energy $\Sigma_{b_{\bar{\alpha}}}$ depicted in Fig. 8b. The renormalization factors are determined such that they cancel the $\frac{1}{2\bar{r}}$ pole in the self-energies minimally and render the inverse Green's function finite. We thus find

$$Z_f = 1 - K \frac{g^2}{2\bar{r}}, \quad Z_b = 1 - N \frac{g^2}{2\bar{r}}. \quad (29)$$

The mass counter-terms are given by the real parts of the self-energies

$$\delta\lambda_f = K g^2 \mu^{2\bar{r}} \frac{\Lambda^r}{r}, \quad \delta\lambda_b = N g^2 \mu^{2\bar{r}} \frac{\Lambda^r}{r}. \quad (30)$$

To one-loop order, there is no vertex renormalization of g , hence we have $Z_g=1$ at this order (note that a g^3

diagram does not exist due to the directed nature of the propagators). The beta function

$$\beta(g) \equiv \mu \frac{dg}{d\mu} \quad (31)$$

can now be obtained by taking the logarithmic μ derivative of Eq. (25). Since $\mu \frac{dg_0}{d\mu} = 0$ we can solve for $\beta(g)$ and finally obtain

$$\beta(g) = -\frac{1-r}{2}g + \frac{K+N}{2}g^3 \quad (32)$$

to one-loop order. One can also consider the flow away from criticality, i.e. the flow of the renormalized tuning parameter ε using S^2 insertions. The resulting correlation lengths exponent is given in Eq. (38) below.

C. $r_{\max} < r < 1$

For $r < 1$ the trivial fixed point $g^* = 0$ is unstable, and the critical properties are instead controlled by an interacting fixed point (labelled ACR) at

$$g^{*2} = \frac{1-r}{K+N} \quad (33)$$

with anomalous field dimensions

$$\eta_b = \beta(g) \left. \frac{d \ln Z_b}{dg} \right|_{g^*} = N g^{*2} \quad (34)$$

$$\eta_f = \beta(g) \left. \frac{d \ln Z_f}{dg} \right|_{g^*} = K g^{*2}. \quad (35)$$

The corresponding RG flow diagram is displayed in Fig. 2c.

ACR describes a quantum phase transition below its upper-critical dimension. As a result, low-energy observables calculated at and near ACR will be fully universal, i.e., cutoff-independent, and hyperscaling is fulfilled.

D. $r \geq 1$

For all $r \geq 1$, i.e., above the upper-critical dimension, the phase transition between LM and LM' is now controlled by the non-interacting FImp fixed point at $g = \varepsilon = 0$. Hence, for all $r > 1$ the phase transition is a level crossing with perturbative corrections – this results e.g. in a jump of the order parameter $T\chi_{\text{loc}}$ (see below), i.e., the transition is formally of first order. Consequently, hyperscaling is violated, and all observables will depend upon the UV cutoff.

For the marginal case, $r = 1$, we expect a logarithmic flow of the marginally irrelevant hybridization g , characteristic of the behavior at the upper-critical dimension. The RG beta function

$$\beta(g) = \frac{K+N}{2}g^3 \quad (36)$$

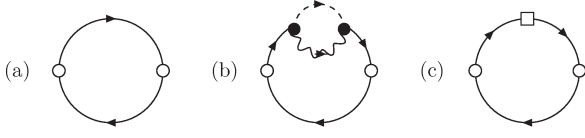


FIG. 9: Feynman diagrams entering $\langle \chi_{\text{loc}} \rangle_{\lambda_0}$ up to quadratic order in g_0 . Open circles are sources, and the blank boxes denotes the counter terms $\delta\lambda_f$. Notation otherwise as in Fig. 8

can be integrated (recall $\beta(g) \equiv \frac{dg}{d \ln \ell}$ where ℓ describes the reduction of the UV cutoff $\Lambda \rightarrow \ell\Lambda$) to give

$$g^2(\ell) = \frac{g_0^2}{1 - (K + N)g_0^2 \ln \ell} \quad (37)$$

with $g(\ell=1) = g_0$. This result can be used to determine logarithmic corrections to observables.

E. Observables near criticality

1. Correlation-length exponent

We start with the correlation-length exponent, ν , of the ACR fixed point. This exponent describes the vanishing of the characteristic crossover temperature in the vicinity of the critical point $T^* \propto (\varepsilon - \varepsilon^*)^\nu$. The lowest-order result for ν , which can be obtained either using the field-theoretic RG scheme via composite operator insertions or using the familiar momentan shell scheme, is

$$\frac{1}{\nu} = r + \mathcal{O}(\bar{r}^2) \quad (r < 1). \quad (38)$$

For $r \geq 1$ the transition is a level crossing, formally $\nu = 1$.

2. Local susceptibility

The local susceptibility $\chi_{\text{loc}} = \chi_{\text{imp,imp}}$ at the critical point follows the scaling behavior $\chi_{\text{loc}} \propto T^{-1+\eta_\chi}$ with an anomalous exponent η_χ . To obtain the corrections to the tree-level result $\chi_{\text{loc}} \propto T^{-1}$ we introduce a χ_{loc} renormalization factor Z_χ from which one obtains the anomalous exponent according to

$$\eta_\chi = \beta(g) \left. \frac{d \ln Z_\chi}{dg} \right|_{g^*}. \quad (39)$$

We determine Z_χ by calculating $\langle \chi_{\text{loc}} \rangle$ directly using perturbative corrections up to quadratic order in g_0 . The corresponding diagrams entering $\langle \chi_{\text{loc}} \rangle_{\lambda_0}$ are given in Fig. 9. In terms of the renormalized coupling constant g

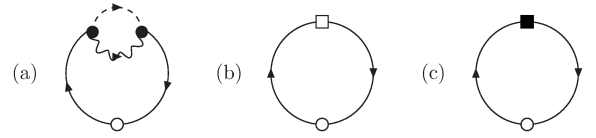


FIG. 10: Feynman diagrams entering the corrections to the unperturbed part of $\langle \hat{Q} \rangle_{\lambda_0}$ up to quadratic order in g_0 . Notation as in the previous figures. Black boxes denote the counter terms $\delta\lambda_b$.

we find at the energy scale $\mu = T$

$$\langle \chi_{\text{loc}} \rangle_{\lambda_0} = e^{-\frac{\lambda_0}{T}} \left(\frac{1}{2T} + \frac{Kg^2}{T} \int_0^{\frac{\Lambda}{T}} dx \frac{x^r}{x^3} \left[2 \tanh \frac{x}{2} + \frac{x^2}{2} \tanh \frac{x}{2} - x - \frac{x^2}{2} \right] \right). \quad (40)$$

Furthermore, the denominator $\langle \hat{Q} \rangle_{\lambda_0}$ receives corrections from the diagrams in Fig. 10, resulting in

$$\langle \hat{Q} \rangle_{\lambda_0} = (N + K)e^{-\frac{\lambda_0}{T}} + 2NKg^2 e^{-\frac{\lambda_0}{T}} \int_0^{\frac{\Lambda}{T}} dx \frac{x^r}{x} \left[\tanh \frac{x}{2} - 1 \right]. \quad (41)$$

The local susceptibility χ_{loc} can then be directly obtained by Eq. (19). The renormalization factor Z_χ is then determined, using minimal subtraction of poles, in an expansion in \bar{r} as

$$Z_\chi = 1 - Kg^2 \frac{1}{\bar{r}} \quad (42)$$

and from this we can directly deduce the anomalous exponent of the local spin susceptibility

$$\eta_\chi^{(\text{spin})} = 2Kg^{*2} = \frac{2K}{K+N}(1-r). \quad (43)$$

The expression for $\eta_\chi^{(\text{flavor})}$ follows by the replacement $K \leftrightarrow N$.

Above the upper-critical dimension, $r > 1$, we simply have $\eta_\chi = 0$ and, thus, $\chi_{\text{loc}}^{(\text{spin})}, \chi_{\text{loc}}^{(\text{flavor})} \propto T^{-1}$ or $\propto \omega^{-1}$. For the marginal case $r = 1$, a calculation analogous to that in Ref. 21, using Eq. (37), gives

$$\chi_{\text{loc}}^{(\text{spin})} \propto \frac{1}{\omega |\ln \omega|^{2K/(K+N)}} \quad (r = 1). \quad (44)$$

3. Order parameter

Inside the stable phases LM and LM', χ_{loc} can be used to define an order parameter for the quantum phase transition: $T\chi_{\text{loc}}^{\text{spin}}$ is finite (zero) for $\varepsilon_0 < 0$ ($\varepsilon_0 > 0$), similarly $T\chi_{\text{loc}}^{(\text{flavor})}$ is finite (zero) for $\varepsilon_0 > 0$ ($\varepsilon_0 < 0$). Approaching

the critical point, both order parameters vanish continuously according to

$$\begin{aligned} T\chi_{\text{loc}}^{(\text{spin})} &\propto (-\varepsilon_0)^{\nu\eta_{\chi}^{(\text{spin})}}, \\ T\chi_{\text{loc}}^{(\text{flavor})} &\propto \varepsilon_0^{\nu\eta_{\chi}^{(\text{flavor})}} \end{aligned} \quad (45)$$

for $r < 1$, which follows e.g. from hyperscaling. Note that these order parameters display a jump upon crossing the transition for $r > 1$.

4. Impurity susceptibility

The evaluation of the impurity susceptibility χ_{imp} to second order in g_0 requires the summation of further diagrams as depicted in Fig. 11. In terms of the renormalized coupling g we obtain

$$\begin{aligned} 2\langle\chi_{\text{b,imp}}\rangle_{\lambda_0} &= \frac{Kg^2}{T} e^{-\frac{\lambda_0}{T}} \int_0^{\frac{\Lambda}{T}} dx \frac{x^r}{x^3} \left[x + \frac{x}{\cosh^2 \frac{x}{2}} \right. \\ &\quad \left. - 4 \tanh \frac{x}{2} \right], \end{aligned} \quad (46)$$

and

$$\begin{aligned} \langle\chi_{\text{b,b}}\rangle_{\lambda_0} - \langle\chi_{\text{b,b}}^0\rangle_{\lambda_0} &= \frac{Kg^2}{T} e^{-\frac{\lambda_0}{T}} \int_0^{\frac{\Lambda}{T}} dx \frac{x^r}{x^3} \left[2 \tanh \frac{x}{2} \right. \\ &\quad \left. - \frac{x}{\cosh^2 \frac{x}{2}} - \frac{x^2 \tanh \frac{x}{2}}{2 \cosh^2 \frac{x}{2}} \right]. \end{aligned} \quad (47)$$

Collecting all contributions to χ_{imp} to second order in g the poles present in the χ_{loc} diagrams cancel and the remaining momentum integrals are UV convergent for $r < 1$. Performing these integrals for $r < 1$ the impurity susceptibility reads

$$\begin{aligned} T\chi_{\text{imp}}^{(\text{spin})} &= \frac{1}{2(N+K)} \left[1 - g^2 K \left(1 + \ln 4 - \frac{2N}{N+K} \ln 4 \right) \right] \\ &\quad + \mathcal{O}(g^4). \end{aligned} \quad (48)$$

As above, the expression for $T\chi_{\text{imp}}^{(\text{flavor})}$ follows by the replacement $K \leftrightarrow N$. With the value of the coupling at the ACR fixed point (33) we finally find for $N = K = 2$, to leading order in $(1-r)$,

$$T\chi_{\text{imp}}^{(\text{spin})} = \begin{cases} \frac{1}{8} - \frac{1}{16}(1-r) + \mathcal{O}(\bar{r}^2) & (r < 1) \\ \frac{1}{8} & (r \geq 1) \end{cases}, \quad (49)$$

with $T\chi_{\text{imp}}^{(\text{flavor})} = T\chi_{\text{imp}}^{(\text{spin})}$ due to the emergent Z_2 symmetry (4). A comparison to NRG data is in Fig. 3. Note that $T\chi_{\text{imp}}$ receives only weak additive logarithmic corrections at $r = 1$; multiplicative logs as in χ_{loc} are absent here. The same applies to S_{imp} below.

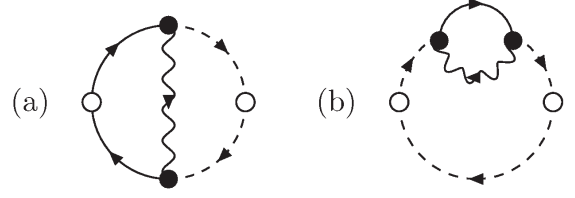


FIG. 11: Further Feynman diagrams entering corrections to the impurity susceptibility to quadratic order in g_0 . Notation as in the previous figures.

5. Impurity entropy

The impurity contribution to the entropy can be obtained from the thermodynamic potential Ω_{imp} by $S_{\text{imp}} = -\partial_T \Omega_{\text{imp}}$. At the FImp fixed point the entropy is $S_{\text{imp}} = \ln(N+K)$, and the lowest-order correction is computed by expanding the thermodynamic potential in the renormalized hybridization g . Note that this correction vanishes for $r \geq 1$, as $g^* = 0$ there. Here, we write the partition function in the physical sector of the Hilbert space ($\hat{Q} = 1$) as³⁷

$$\frac{Z_{\text{imp}}}{Z_{\text{imp},0}} = \lim_{\lambda_0 \rightarrow \infty} \frac{\langle \hat{Q} \rangle_{\lambda_0}}{\langle \hat{Q} \rangle_{\lambda_0,0}}, \quad (50)$$

where $\langle \dots \rangle_{\lambda_0,0}$ is the expectation value in the presence of λ_0 without coupling to the bath. The thermodynamic potential is given by

$$\Omega_{\text{imp}} - \Omega_{\text{imp},0} = -T \ln \frac{Z_{\text{imp}}}{Z_{\text{imp},0}}. \quad (51)$$

The correction to $\langle \hat{Q} \rangle_{\lambda_0}$ due to the coupling to the bath up to quadratic order in g has already been calculated in Eq. (41) which enables us now to directly evaluate Eq. (51). Taking the temperature derivative of the resulting expression and evaluating the remaining integral in the limit $T \rightarrow 0$ and $r \rightarrow 1$ we obtain

$$S_{\text{imp}} = \ln(K+N) - g^2 \frac{4NK}{N+K} \ln 2 + \mathcal{O}(g^4). \quad (52)$$

As expected, the entropy correction is fully universal and finite in the limit $T \rightarrow 0$. Note that in higher-order terms of the diagrammatic expansion for the thermodynamic potential Ω_{imp} disconnected diagrams appear.³⁷

Finally, inserting the fixed-point value of the coupling g into Eq. (52), we find the impurity entropy in the two-channel case $N = 2$ and $K = 2$ to be

$$S_{\text{imp}} = \begin{cases} \ln 4 - (1-r) \ln 2 + \mathcal{O}(\bar{r}^2) & (r < 1) \\ \ln 4 & (r \geq 1) \end{cases}. \quad (53)$$

Comparison with the numerical result again shows very good agreement, Fig. 4.

6. Conduction-electron T matrix

For the single-channel pseudogap Kondo problem, it has been shown that the conduction-electron T matrix $T(\omega)$ displays a power-law divergence of the form $T(\omega) \propto |\omega|^{-r}$ at all intermediate-coupling fixed points.^{20,21} Analytically, this follows – for all perturbative expansions – from the diagrammatic structure of the T matrix (or, alternatively, from a Ward identity).

In the two-channel case, we find the same qualitative arguments to apply, i.e., at the NFL, SCR, and ACR fixed points the T matrix obeys the exact result

$$T(\omega) \propto |\omega|^{-r} \quad (r < 1). \quad (54)$$

At one-loop level, an explicit calculation gives $\eta_T = (K + N)g^2$ which yields $\eta_T = 1 - r$ as expected. For $r > 1$, $\text{Im}T(\omega) \propto \delta(\omega)$.

For $r = 1$, the logarithmic flow of the coupling, Eq. (37), can be used to deduce $T(\omega) \propto 1/(\omega |\ln \omega|)$ which gives

$$\text{Im}T(\omega) \propto \frac{1}{\omega |\ln \omega|^2} \quad (55)$$

in analogy to Ref. 21.

VI. CONCLUSIONS

We have explored the two-channel Kondo effect for magnetic impurities embedded into a fermionic host with a power-law pseudogapped density of states. We have determined the phase diagram as function of the DOS exponent r and discussed the boundary quantum phase transitions of the relevant Kondo and Anderson models. These transitions are described by fermionic (as opposed to usual bosonic) quantum field theories; from their properties we conclude that there is no underlying CFT description.

Our results demonstrate the versatility of the Anderson-model epsilon expansions developed in Refs. 20,21: Those have not only allowed a full understanding of the critical behavior of the single-channel ($S = 1/2$) pseudogap Kondo problem, but also of the corresponding underscreened⁴⁷ and overscreened pseudogap Kondo models (this work). Further applications, e.g., to multi-impurity models, appear possible. Also, the Anderson-model formulation should enable studies of non-equilibrium dynamics of pseudogap Kondo problems.

Our results are of potential relevance to two-channel impurities in unconventional superconductors and in graphene; for the latter case the extension of the present calculations to finite bias⁴⁸ is an interesting future topic.

Acknowledgments

We thank A. J. Schofield and, in particular, K. Ingersent for helpful discussions. This research has been supported by the Deutsche Forschungsgemeinschaft through SFB 608 (LF), FOR 960 (AB, MV), and AN 275/6-2 (FBA). FBA and MV also acknowledge support from the German-Israeli-Foundation.

Appendix A: Compactified σ - τ Kondo model and O(3)-symmetric Anderson model

Here we briefly discuss an alternative formulation of the two-channel Kondo model which eventually leads to a theory of non-interacting Majorana fermions.

1. Metallic bath, $r=0$

The low-energy physics of the standard two-channel Kondo problem ($r = 0$) has been argued to be equivalent to that of the so-called σ - τ Kondo model – this is a “compactified” single-channel Kondo model where the roles of the two screening channels are taken by spin and a charge pseudospin.^{49,50} The corresponding Hamiltonian can be expressed as

$$\mathcal{H}_{\sigma-\tau} = [J_1 \vec{\sigma}(0) + J_2 \vec{\tau}(0)] \cdot \vec{S} + \int_{-\Lambda}^{\Lambda} dk k c_{k\sigma}^\dagger c_{k\sigma} \quad (\text{A1})$$

where, as above, \vec{S} is a spin-1/2 SU(2) spin and we have represented the bath by linearly dispersing chiral fermions $c_{k\sigma}$. Spin degrees of freedom $\sigma = \uparrow, \downarrow$ are implicitly summed. The conduction electron spin $\vec{\sigma}(0)$ and pseudospin $\vec{\tau}(0)$ are defined as

$$\vec{\sigma}(0) = (c_{\uparrow}^\dagger(0), c_{\downarrow}^\dagger(0)) \cdot \vec{\tau} \cdot \begin{pmatrix} c_{\uparrow}(0) \\ c_{\downarrow}(0) \end{pmatrix} \quad (\text{A2})$$

$$\vec{\tau}(0) = (c_{\uparrow}^\dagger(0), c_{\downarrow}(0)) \cdot \vec{\tau} \cdot \begin{pmatrix} c_{\uparrow}(0) \\ c_{\downarrow}^\dagger(0) \end{pmatrix}, \quad (\text{A3})$$

where $c_\sigma(0) = \int dk c_{k\sigma}$. Interestingly, the low-energy physics of the σ - τ Kondo model is described by a fixed point with non-Fermi liquid behavior which is located at *strong* coupling, not at intermediate coupling as in the two-channel Kondo problem. The equivalence of the two-channel Kondo model and the σ - τ Kondo model has been established using bosonization and conformal field theory techniques.^{49–51}

The nature of the low-energy non-Fermi liquid becomes transparent by considering the so-called O(3)-symmetric Anderson model which displays an anomalous hybridization term. Its Hamiltonian is given by

$\mathcal{H}_{O(3)} = \mathcal{H}_{1cA} + \mathcal{H}_{\text{ahyb}}$ with

$$\mathcal{H}_{1cA} = U \left(n_{f\uparrow} - \frac{1}{2} \right) \left(n_{f\downarrow} - \frac{1}{2} \right) + \int_{-\Lambda}^{\Lambda} dk k c_{k\sigma}^\dagger c_{k\sigma} + g_0 \sum_{\sigma} [f_{\sigma}^\dagger c_{\sigma}(0) + \text{H.c.}], \quad (\text{A4})$$

$$\mathcal{H}_{\text{ahyb}} = -g_a \left[f_{\downarrow}^\dagger c_{\downarrow}^\dagger(0) + f_{\downarrow}^\dagger c_{\downarrow}(0) + \text{H.c.} \right], \quad (\text{A5})$$

where f_{σ}^\dagger creates the localized impurity state with spin σ and $n_{f\sigma} = f_{\sigma}^\dagger f_{\sigma}$. Note that the chemical potential on the impurity site has been chosen such that the model is p-h symmetric. In the Kondo limit, the O(3)-symmetric Anderson model maps onto the σ - τ Kondo model.⁵¹

Appealing to the adiabatic continuity between the $U = 0$ and large- U limits in this Anderson model suggests to discuss the weakly-interacting case. The Hamiltonian $\mathcal{H}_{O(3)}$ can be conveniently re-written in terms of Majorana fermions:

$$\mathcal{H}_{O(3)} = U d_1 d_2 d_3 d_0 + i \sum_{\alpha=0}^3 \int_{-\Lambda}^{\Lambda} dk k \psi_{-k\alpha} \psi_{k\alpha} + i g_0 \sum_{\alpha=1}^3 \psi_{\alpha}(0) d_{\alpha} + i(g_0 - 2g_a) \psi_0(0) d_0. \quad (\text{A6})$$

Here, the impurity Majorana fermions are defined by

$$f_{\uparrow} = \frac{1}{\sqrt{2}}(d_1 - i d_2), \quad f_{\downarrow} = \frac{1}{\sqrt{2}}(-d_3 + i d_0), \quad (\text{A7})$$

where $d_{\alpha}^\dagger = d_{\alpha}$ and $\{d_{\alpha}, d_{\beta}\} = \delta_{\alpha,\beta}$ for $\alpha = 0, 1, 2, 3$. The Majorana fermions for the conduction electrons are defined similarly⁵¹ which in Fourier space reads

$$c_{k\uparrow} = \frac{1}{\sqrt{2}}(-i\psi_{k1} - \psi_{k2}), \quad c_{k\downarrow} = \frac{1}{\sqrt{2}}(i\psi_{k3} - \psi_{k4}) \quad (\text{A8})$$

with $\psi_{k\alpha}^\dagger = \psi_{-k\alpha}$. Remarkably, for $2g_a = g_0$ the impurity couples only via d_{α} for $\alpha = 1, 2, 3$ to the conduction Majorana fermions while d_0 remains free.

The Hamiltonian in Eq. (A6) is in particular suitable to study thermodynamic quantities. Note that for $U = 0$ the model is exactly solvable and the impurity Green's functions $G_{\alpha}(\tau) = -\langle T_{\tau} d_{\alpha}(\tau) d_{\alpha}(0) \rangle$ are known exactly. For $U = 0$ and $2g_a = g_0$, their Fourier counterparts read

$$G_0(i\omega_n) = \frac{1}{i\omega_n}, \quad G_{\alpha}(i\omega_n) = \frac{1}{i\omega_n + iA_0 \text{sgn}(\omega_n)}, \quad (\text{A9})$$

for $\alpha = 1, 2, 3$. Here, we have introduced $A_0 = \pi g_0^2$.

A straightforward calculation now shows then that there is a residual impurity entropy $S_{\text{imp}} = \frac{1}{2} \ln 2$ of a free Majorana fermion.⁵² By adiabatic continuity, this entropy persists into the regime of large U and then corresponds to the entropy of the overscreened two-channel Kondo impurity.

2. Pseudogap bath

The obvious question is whether the σ - τ Kondo and O(3)-symmetric Anderson models continue to represent the physics of the two-channel Kondo problem for a pseudogap bath DOS with $r > 0$. To answer this, let us consider the non-interacting limit and $2g_a = g_0$ of the O(3) Anderson model. The Green's functions in Eq. (A9) for $\omega_n/\Lambda \ll 1$ are now given by²¹

$$G_0(i\omega_n) = \frac{1}{i\omega_n}, \quad (\text{A10})$$

$$G_{\alpha}(i\omega_n) = \frac{1}{i\omega_n + iA_0 \text{sgn}(\omega_n) |\omega_n|^r} \quad (\text{A11})$$

for $\alpha = 1, 2, 3$. They yield an impurity entropy of

$$S_{\text{imp}} = \frac{1}{2} \ln 2 + \frac{3}{2} r \ln 2. \quad (\text{A12})$$

and an impurity susceptibility of

$$T\chi_{\text{imp}}(T) = \frac{3r}{32}. \quad (\text{A13})$$

This result is not in agreement with the numerical data in Figs. 3 and 4, which instead are well fitted by $S_{\text{imp}} = \frac{1}{2} \ln 2 + 2r \ln 2$ and $T\chi_{\text{imp}}(T) = \frac{r}{6}$ (Ref. 19). We are forced to conclude that the low-energy behavior of the σ - τ Kondo and O(3)-symmetric Anderson models is *not* identical to that of the two-channel Kondo model once $r > 0$. In other words, the equivalence is restricted to the metallic $r = 0$ case. Given the fact that neither bosonization nor CFT appear to be applicable to the pseudogap Kondo models, this may not come as a surprise.

Let us finish with the remark that an extension of the Majorana resonant-level model that corresponds to the solvable point of the two-channel Kondo model⁷ to a pseudogap DOS also does not yield the numerically found impurity entropy.

¹ P. Nozières and A. Blandin, J. Phys. (Paris) **41**, 193 (1980).

² N. Andrei and C. Destri, Phys. Rev. Lett. **52**, 364 (1984).

³ P. B. Wiegmann and A. M. Tsvelik, Z. Phys. B **54**, 201 (1985).

⁴ I. Affleck and A. W. W. Ludwig, Nucl. Phys. B **352**, 849 (1991); *ibid.* **360**, 641 (1991).

⁵ A. W. W. Ludwig and I. Affleck, Phys. Rev. Lett. **67**, 3160 (1991).

- ⁶ E. Sela, A. K. Mitchell, and L. Fritz, Phys. Rev. Lett. **106**, 147202 (2011).
- ⁷ V. Emery and S. Kivelson, Phys. Rev. B **46**, 10812 (1992).
- ⁸ D. L. Cox and A. Zawadowski, Adv. Phys. **47**, 599 (1998).
- ⁹ D. L. Cox, Phys. Rev. Lett. **59**, 1240 (1987); *ibid.* **61**, 1527(E) (1988).
- ¹⁰ A. Schiller, F. B. Anders, and D. L. Cox, Phys. Rev. Lett. **81**, 3235 (1998).
- ¹¹ R. M. Potok, I. G. Rau, H. Shtrikman, Y. Oreg, and D. Goldhaber-Gordon, Nature **446**, 167 (2007).
- ¹² Y. Oreg and D. Goldhaber-Gordon, Phys. Rev. Lett. **90**, 136602 (2003).
- ¹³ H. C. Manoharan *et al.*, (unpublished).
- ¹⁴ A. C. Hewson, *The Kondo Problem to Heavy Fermions*, Cambridge University Press, Cambridge (1997).
- ¹⁵ D. Withoff and E. Fradkin, Phys. Rev. Lett. **64**, 1835 (1990).
- ¹⁶ C. R. Cassanello and E. Fradkin, Phys. Rev. B **53**, 15079 (1996) and **56**, 11246 (1997).
- ¹⁷ A. Polkovnikov, Phys. Rev. B **65**, 064503 (2002).
- ¹⁸ R. Bulla, T. Pruschke, and A. C. Hewson, J. Phys.: Condens. Matter **9**, 10463 (1997); R. Bulla, M. T. Glossop, D. E. Logan, and T. Pruschke, *ibid.* **12**, 4899 (2000).
- ¹⁹ C. Gonzalez-Buxton and K. Ingersent, Phys. Rev. B **57**, 14254 (1998).
- ²⁰ M. Vojta and L. Fritz, Phys. Rev. B **70**, 094502 (2004).
- ²¹ L. Fritz and M. Vojta, Phys. Rev. B **70**, 214427 (2004).
- ²² K. Sengupta and G. Baskaran, Phys. Rev. B **77**, 045417 (2007).
- ²³ Ref. 19 overlooked the slow flow of the particle-hole asymmetry towards zero in the NFL phase for $0 < r < r_{\max}$ (K. Ingersent, private communication). As a result, the phase diagram in Fig. 30a of Ref. 19 differs qualitatively from ours (Fig. 1b).
- ²⁴ The fixed point LM' was labelled ASC (for asymmetric strong coupling) in Ref. 19.
- ²⁵ C. J. Bolech and N. Andrei, Phys. Rev. Lett. **88**, 237206 (2002).
- ²⁶ H. Johannesson, N. Andrei, and C. J. Bolech, Phys. Rev. B **68**, 075112 (2003).
- ²⁷ C. J. Bolech and N. Andrei, Phys. Rev. B **71**, 205104 (2005).
- ²⁸ F. B. Anders, Phys. Rev. B **71**, 121101(R) (2005).
- ²⁹ G. R. Stewart, Z. Fisk, and J. O. Willis, Phys. Rev. B **28**, 172 (1983).
- ³⁰ F. G. Aliev, H. El Mfarrej, S. Vieira, R. Villar, and J. L. Martinez, Europhys. Lett. **32**, 765 (1995).
- ³¹ K. A. Matveev, Sov. Phys. JETP **72**, 892 (1991).
- ³² E. Lebanon, A. Schiller, and F. B. Anders, Phys. Rev. B **68**, 041311(R) (2003).
- ³³ O. Parcollet and A. Georges, Phys. Rev. Lett. **79**, 4665 (1997); O. Parcollet, A. Georges, G. Kotliar, and A. M. Sengupta, Phys. Rev. B **58**, 3794 (1998).
- ³⁴ M. Vojta, Phys. Rev. Lett. **87**, 097202 (2001).
- ³⁵ M. Vojta, Phil. Mag. **86**, 1807 (2006).
- ³⁶ M. Vojta, C. Buragohain and S. Sachdev, Phys. Rev. B **61**, 15152 (2000).
- ³⁷ M. Kirčan and M. Vojta, Phys. Rev. B **69**, 174421 (2004).
- ³⁸ H. Georgi, *Lie Algebras in Particle Physics*, Westview Press, Boulder (1999).
- ³⁹ R. Bulla, T. A. Costi, and T. Pruschke, Rev. Mod. Phys. **80**, 395 (2008).
- ⁴⁰ I. Affleck and A. W. W. Ludwig, Phys. Rev. Lett. **67**, 161 (1991).
- ⁴¹ S. Florens and A. Rosch, Phys. Rev. Lett. **92**, 216601 (2004).
- ⁴² P. W. Anderson, J. Phys. C **3**, 2436 (1970).
- ⁴³ E. Brezin, J. C. Le Guillou, and J. Zinn-Justin, in *Phase transitions and critical phenomena*, eds. C. Domb and M. S. Green, Page Bros. , Norwich (1996), Vol. 6.
- ⁴⁴ M. Le Bellac, *Quantum and Statistical Field Theory*, Oxford University Press, Oxford (1992).
- ⁴⁵ A. Zawadowski and P. Fazekas, Z. Physik **226**, 235 (1969); P. Coleman, Phys. Rev. B **29**, 3035 (1984).
- ⁴⁶ T. A. Costi, J. Kroha, and P. Wölfle, Phys. Rev. B **53**, 1850 (1996).
- ⁴⁷ S. Florens and M. Vojta, Phys. Rev. B **72**, 115117 (2005).
- ⁴⁸ M. Vojta, L. Fritz, and R. Bulla, EPL **90**, 27006 (2010).
- ⁴⁹ P. Coleman and A. J. Schofield, Phys. Rev. Lett. **75**, 2184 (1995).
- ⁵⁰ A. J. Schofield, Phys. Rev. B **55**, 5627 (1997).
- ⁵¹ R. Bulla, A. C. Hewson, and G. M. Zhang, Phys. Rev. B **56**, 11721 (1997).
- ⁵² G. M. Zhang and A. C. Hewson, Phys. Rev. B **54**, 1169 (1996).